

Unlocking Mode Programming with Multi-Plane Light Conversion Using Computer-Generated Hologram Optimisation

Stefan Rothe^{a,e}, Fabio Barbosa^b, Jürgen W. Czarske^{c,d,f}, Filipe M. Ferreira^{b,g}

^aDepartment of Applied Physics, Yale University, New Haven, CT 06520, USA

^bOptical Networks, Dept Electronic & Electrical Eng, University College London, UK

^cTU Dresden, Faculty of Electrical and Computer Engineering, Laboratory of Measurement and Sensor System Technique, 01062 Dresden, Germany

^dTU Dresden, Faculty of Physics, 01062 Dresden, Germany

^estefan.rothe@yale.edu

^fjuergen.czarske@tu-dresden.de

^gf.ferreira@ucl.ac.uk

Keyword: Spatial Light Modulator, wavefront shaping, Optimisation, Direct Search, Multi-Plane Light Conversion, Wavefront Matching

Abstract: Programmable optical devices provide performance enhancement and flexibility to spatial multiplexing systems enabling transmission of tributaries in high-order eigenmodes of spatially-diverse transmission media, like multimode fibre (MMF). Wavefront shaping with spatial light modulators (SLMs) facilitates scalability of the transmission media by allowing for channel diagonalization and quasi-single-input single-output operation. Programmable mode multiplexing configurations like multi-plane light conversion (MPLC) utilise the SLM and offer the potential to simultaneously launch an arbitrary subset of spatial tributaries in any N -mode MMF. Such programmable optical processor would enable the throughput of space-division multiplexing (SDM) systems to be progressively increased by addressing a growing number of tributaries over one MMF and in this way meet a growing traffic demand – similarly to the wavelength-division multiplexing evolution path. Conventionally, MPLC phasemasks are calculated using the wavefront matching algorithm (WMA). However, this method does not exploit the full potential of programmable mode multiplexers. We show, that computer-generated hologram algorithms like direct search enable significant improvement compared to the traditional WMA-approach. Such gains are enabled by tailored cost functions with dynamic constraints concerning insertion loss as well as mode extinction ratio. We show that average mode extinction ratio can be greatly improved by as much as ≈ 15 dB at the expense of insertion loss deterioration of < 3 dB. One particular feature of programmable mode multiplexers is the adaptability to optimised transmission functions. Besides conventional LP modes transmission, we employ our approach on Schmidt modes, which are spatial eigenchannels with minimum crosstalk derived from a measured transmission matrix.

1. Introduction

SDM is an established approach to overcome the capacity exhaustion in optical single-mode fibre networks that underlie the nonlinear Shannon-limit [1, 2, 3, 4]. Amongst SDM implementation options, the approach based on MMFs allows the highest information density and consequently the highest efficiency gains regarding array integration in transceivers and other network elements. Usually, undesired effects in SDM operation with MMF such as group delay spread [5], and crosstalk [6] are compensated on the receiver-side via multiple-input multiple-output (MIMO)-digital signal processing (DSP) [7, 8]. Other effects such as mode-dependent loss (MDL) [9] require advanced detection algorithms [10]. Furthermore, the group delay spread and the MDL loss have been mitigated through the cyclic mode-group permutation technique [11] making all information tributaries to have similar spreading reducing the memory depth of MIMO-DSP.

The linear crosstalk in MMF is due to linear mode coupling, refractive-index inhomogenities or small deviations of the core-cladding boundary caused by perturbations introduced during the fabrication process or by

mechanical stresses imposed on the MMF field. These imperfections cause the MMF modes to couple among each other. As such, when exciting a pure mode at the MMF input, some of its power is scattered to other guided modes. This power transfer results in a spreading of the channel impulse response due to characteristic group velocity [6]. Therefore, the equalisation of the received signal must span over a time window that covers all the significant distortions undergone by a given information symbol. The ultimate objective of this process is to end up with the lowest possible crosstalk after equalization, or in positive terms, the highest possible mode extinction ratio (MER).

The complexity required on the receiver-side increases significantly with the number of modes used. Despite the number of information tributaries M actually transmitted, all N fibre modes need to be detected such that MIMO-DSP can be performed, otherwise MDL would lead to frequent outage in the presence of non-negligible linear crosstalk. This leads to a complexity increase not only in terms of computational complexity (where MIMO complexity scales with N^2), but also in terms of hardware with the number of coherent receiver front-ends required being equal to the number of fibre modes N [12]. While MMFs provide great potential for spatial multiplexing efficiency gains, with as much as $N = 1000$ modes [13], is what makes this particularly critical, since it would not be feasible to have N coherent front-ends at system beginning-of-life but only at system end-of-life.

Here, we propose a programmable optical processor enabling scaling the number of information tributaries over an optical fibre with $N > M$ to progressively exploit the fibre spatial domain – similar to the successful development of wavelength division multiplex systems with multiple wavelength channels as traffic demand grows. Using channel knowledge through, for example, the optical transmission matrix [14, 15, 16, 17, 18, 19, 20, 21, 22, 23] and a programmable mode multiplexer, one can find the required wavefront that compensates for crosstalk, for a defined sub-domain of spatial modes. In order to transmit such tailored signals to the receiver with high fidelity, precise modulation of the amplitude, and especially the phase of the input wavefront for each desired spatial mode is necessary. Here, we neglect any polarisation mixing in the MMF.

Photonic lanterns are fused-fibre devices that map a 1D spot array (or another arrangement of non-overlapping spots) provided by a collection of single-mode fibre (SMF) to a 2D superposition of spatial modes interfacing an MMF [24]. The underlying approach is to form a multimode waveguide by gradually transition the SMF array/bundle into a composite multimode waveguide [25]. There are several fabrication processes that all aim to conserve entropy allowing for a nearly lossless transition. As a result, photonic lanterns provide perhaps the highest optical coupling efficiency of usually less than 1 dB insertion loss (IL), which makes it particularly promising for photon sensitive applications such as quantum networks [26, 27]. However, the photonic lantern suffers from limitations in its reconfigurability. Although there are solutions reporting a mode-selective transmission of a few, e.g. 6 modes over a comparably short MMF length of 100 m [28], the *programmability* is largely limited before, and even impossible after the photonic lantern has been fabricated. In particular, mitigation of degenerate mode coupling turns out to represent the major hurdle and can hardly be achieved despite clever SMF arrangement or microstructured preforms for large mode numbers above 15 [29, 30]). This limits the achievable selectivity to the mode-group-level.

The SLM is probably the device that allows for the highest flexibility for modulating the amplitude and phase of a wavefront. Given an SLM and an appropriate wavefront shaping algorithm on the transmitter-side, any tailored signal, i.e. any arbitrary mode combination can be provided to the receiver [31, 32, 33]. For instance Schmidt modes [34], also referred to as transmission eigenchannels [15, 35, 36, 37, 38, 32], could be launched and detected in order to pre- and post-compensate, respectively, MMF-induced crosstalk and thus allow (partial) channel diagonalisation. Alternatively, principal modes [39, 40] suffer minimal mode dispersion and distortion. These specific mode sets enable improvement on information density with scalable DSP equalisation complexity [41]. Moreover, mode combinations can be extracted from the transmission matrix generating a confidential data link to a legitimate recipient [42]. Thus, information security, DSP complexity and spatial multiplexing gain can be scaled simultaneously and flexibly with an SLM. The key to high performance is to find the right wavefront building a high-order mode multiplexer transmitting the desired mode combinations associated to M respective spatial sub-channels.

One flexible and high-dimensional mode multiplexing approach which can be realised with an SLM is MPLC [43, 44, 45, 46, 47, 48, 49, 25, 50, 51]. Moreover, MPLC setups are also used for coherent beam combining [52], untangling light that outputs a MMF [53], quantum cryptography [54], computational imaging [55], and diffractive neural networks / optical computing [56, 57, 58]. The MPLC apparatus is an all-optical device that enables mapping of spatially disjoint input spots to spatially overlapping mode fields. In most SDM applications that employ an MPLC, the phasemasks are calculated *a priori* as part of an optimisation procedure based on WMA [59]. The results are displayed on the SLM or etched on a reflective surface performing the desired transformation. In that way, the spatial bandwidth of MMFs can be exploited gainfully achieving data

rates in the Pbit s^{-1} range via only one single core of standard MMF [48].

In the context of a communication system, however, the WMA does not provide a global optimum for average MER, i.e. $\overline{\text{MER}}$, and simultaneously minimum IL. Recent experimental work on multiplexing 250 Hermite-Gaussian (HG) modes in a graded-index MMF shows IL ranging from -3.5 dB to -2.5 dB, and crosstalk ranging from -6.8 dB to -2.1 dB [49]. Even though there are significant experimental breakthroughs involved in these results, the achieved fidelity of the multiplexer cannot be regarded as sufficient to generate specific mode sets that would be required for channel diagonalisation in long MMF transmission links covering hundreds of km. In this paper, we show that by using tailored cost functions, the MPLC fidelity can be significantly improved using computer-generated hologram algorithms [54, 60, 61]. We demonstrate that by scaling the cost function constraints, the degree of optimisation, namely maximum $\overline{\text{MER}}$ and / or minimum IL, can be tuned flexibly. In our simulations, we find that the further optimisation on $\overline{\text{MER}}$ leads to additional reduction of the MDL. In recent work, flexible cost function constraints were employed within a gradient ascent optimisation framework [50]. Here, our approach integrates the traditional WMA into a direct-search environment, leveraging a different optimisation setting. We define the solution space of our approach with respect to the number of tributaries M using a fixed SLM pixel number. Our results enable customised optimisation for high-performance SDM communication systems with high number of utilised spatial channels transmitting linearly polarized (LP) modes, as well as Schmidt modes. This is particularly significant, since recent works focus on shaping HG modes to explore the inherent symmetry of Canonical SLMs and allowing only for mode group selectivity in MMF. In turn, cylindrically symmetric LP modes that are the MMF eigenmodes can be directly addressed by our approach. Therefore, our work contributes to efficient and arbitrary wavefront shaping of cylindrical mode sets using an MPLC device.

2. Parameter selection and starting point

We assume a standard $\varnothing 50 \mu\text{m}$ -core MMF with graded-index: core grading exponent equal to 1.97 and core relative refractive index difference equal to 0.01. Such fibre guides 45 LP modes per polarisation at 1550 nm wavelength. The fibre refractive index profile is shown in Fig. 1a. Although the fabrication of this optical fibre is highly precise, crosstalk is inevitably present after long transmission distance. Usually, MMF exhibits a minimum of -20 dB crosstalk after 100 km transmission. This phenomenon can be traced in Fig. 1b that shows the transmission matrix after 10 km transmission, where off-diagonal entries indicate the presence of crosstalk. For this measurement, we used photonic lantern-based mode (de-)multiplex and standard coherent detection. Most methods compensating crosstalk underlie powerful DSP paradigms applied on the receiver-side, whose computational effort increases exponentially with each added tributary. To allow flexibility gains in SDM systems, however, the number of tributaries should refer to a scalable parameter without causing adverse performance impact. Here, we introduce transmitter-side precompensation using a programmable mode multiplexer, i.e. wavefront shaping with an SLM. Following the MPLC approach reported in Ref. [45], the SLM is being illuminated by $120 \mu\text{m}$ spaced input beams that are arranged in an rectangular array with Gaussian profile and $60 \mu\text{m}$ mode field diameter. Depending on the number of actually used tributaries M , the number of active input beams varies accordingly. We consider a fixed number of $K = 5$ reflection passages (see discussion in Sec. 3) each of which is modeled by simulating a 256×256 pixel grid with $8 \mu\text{m}$ pixels. The passages are connected with a 21 mm free-space propagation kernel. The entire apparatus is modelled in transmission. This being said, effects from input angle misalignment or shadowing of the beam path are neglected. Fig. 1c shows exemplary phasemasks for a $K = 5$ -passage configuration and intensity profiles at the corresponding axial position along the propagation direction z (indicated with a black arrow). The phasemasks shown are the result of our multiplexer design and carry out the desired transformation from $M = 5$ disjoint input beams into the incoherent superposition of 5 output modes.

Within this work, we present a mode multiplexer that achieves greatly improved performance on the aforementioned wavefront shaping task. In this context, there are two crucial parameters we use as cost for optimisation. First, the excitation of each target mode should be as precise as possible. In particular, the output of the mode multiplexer should exhibit as high purity as possible that is the coupling to a target mode calculated as complex spatial overlap integral. At the same time, the overlap to residual modes should be as low as possible achieving minimum crosstalk. In order to quantify the achievable purity of the mode multiplexer, the MER is determined calculating the ratio between the power in the m th mode and the power in all other N modes (i.e. reciprocal representation of crosstalk)

$$\text{MER}_m = 20 \cdot \log_{10} \left(\frac{|\int \int E_m^* E_m|}{\sum_{i \neq m}^N |\int \int E_m^* E_i|} \right), \quad \overline{\text{MER}} = \frac{1}{M} \sum_m^M \text{MER}_m \quad (1)$$

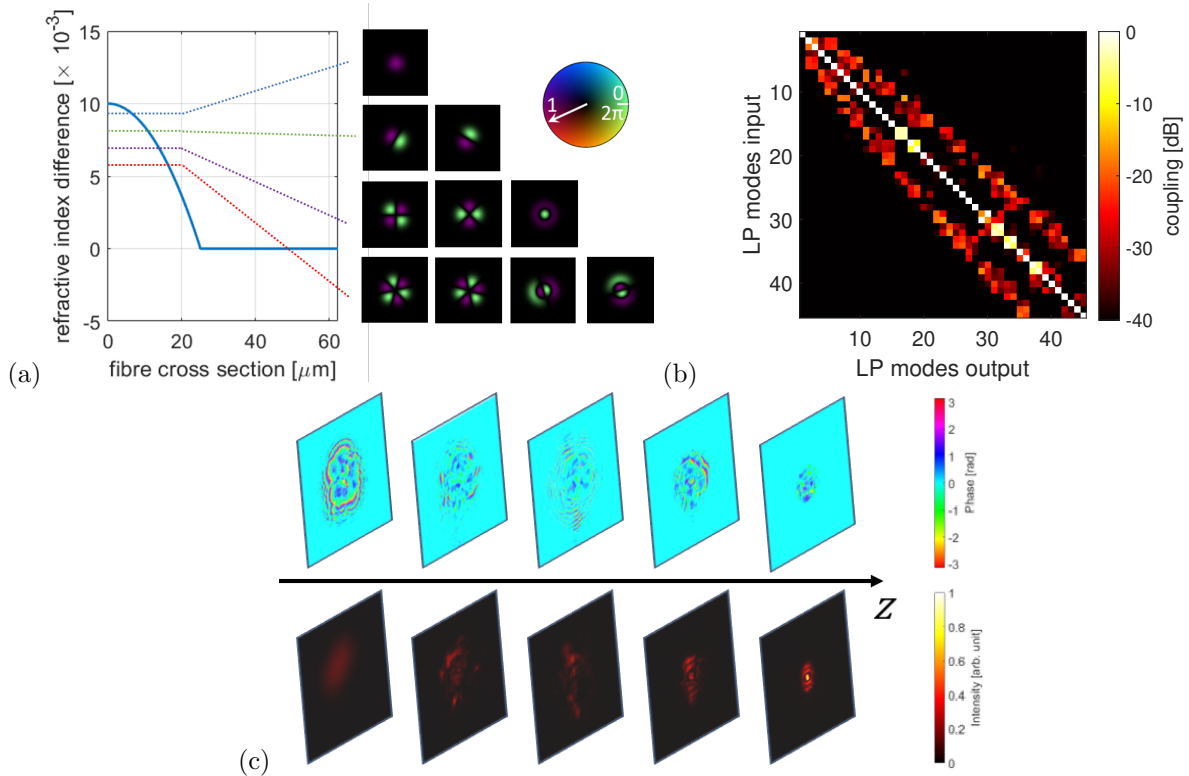


Figure 1: (a) Refractive index profile of the considered MMF. This MMF supports $N = 45$ LP modes per polarisation, of which the first 10 modes corresponding to the first 4 lowest order-groups are shown on the right-hand side. (b) Measured transmission matrix of 10 km MMF using photonic lantern as mode (de-) multiplex and coherent detection. (c) Phasemasks (top) and intensity profiles (bottom) of a simulated $K = 5$ -passage MPLC for $M = 5$ tributaries. We have randomly drawn the target modes from the 45-mode set of the considered MMF. Disjoint Gaussian input spots transition into an incoherent superposition of LP modes at the output by using WMA. We normalised phase (intensity) plots to the same phase (intensity) scale. Colorbars for phase and intensity are shown on the right. We used the code provided in Refs. [45, 62] to produce this result.

where E_m^* is the conjugate mode multiplexer output field in the target LP mode and E_i indicates the field of any other LP mode. As such, performance on coupling efficiency for all M tributaries can be determined by calculating the average $\overline{\text{MER}}$. Second, it is desirable to carry out a power-efficient shaping process. Therefore, we calculate the IL that provides information on how much light is lost from input to output of the multiplexer. We calculate IL by the average singular value s_v of the multiplexer's coupling matrix

$$\text{IL} = 20 \cdot \log_{10}(\overline{s_v}), \quad (2)$$

where the operation $\overline{(\cdot)}$ indicates averaging over all singular values s_v [45]. When transmitting data over spatially parallel paths, equal power distribution, i.e. low mode dependency, is desirable. Therefore, in our simulations we characterise $\text{MDL} = 10 \cdot \log_{10}(s_{v,\max}^2/s_{v,\min}^2)$ [49], yet do not implement it as cost function for optimisation.

3. Implementation of wavefront matching and direct search optimisation

3.1. Wavefront matching

Mode multiplexing for a high number of tributaries has become a pivotal desire. Over the past decade, the MPLC approach has become subject of intense research activities. Depending on both the input spot distribution and target mode profiles, phasemasks are required that enable the desired beam transformation. Usually, the WMA is used to precalculate such phasemasks and it works as follows [59]. We assume propagation along the optical axis z , and define both an input field distribution at the input plane, as well as a target field distribution at the output plane. In between, there are K equally spaced planes at which the forward propagating beam can experience spatial phase modulation. We refer to these planes as (reflection) passages, as in a real

experiment an SLM would induce phase modulation in a reflection configuration. In traditional MPLC setups, the WMA is used to calculate the spatial overlap at each passage between forward propagating input field, e.g. an arrangement of disjoint Gaussian spots, and output target modes propagating in backward direction. The phase conjugate mismatch between spots and modes at each passage is computed and displayed as phase modulation in the following iteration. After a certain number of iteration passes, this algorithm converges to a smooth transition from input field to target output field.

It has been shown that WMA accomplishes high multiplexing throughput with a comparably low number of reflection passages. Such gains in the required number of passages are achieved by harnessing Canonical symmetries in rectangular mode sets such as HG modes that align well on the rectangular pixel grid of an SLM [44, 45, 47]. However, these advantages are specific to systems designed to utilize HG modes.

Here, the focus of our work is on generating LP modes. In rotationally symmetric fibres, LP modes form complete orthogonal set under the scalar approximation, making them the appropriate basis for describing signal propagation [63, 64, 23]. Specifically, for fibres with a parabolic refractive index profile—such as graded-index fibres, the modes are best represented using Laguerre-Gaussian polynomials, often referred to as LG modes. For this reason, LP modes are usually used in experimental demonstrations on high-throughput SDM communications [48].

In turn, HG modes with Canonical symmetries are not inherently suited for rotationally symmetric fibres, or spherical resonator configurations [65], as they do not satisfy the boundary conditions required for cylindrically symmetric fibres. Instead, HG modes are more appropriate for rectangular waveguides or free-space propagation, where their boundary conditions are naturally satisfied.

Our work therefore focuses on the more generally deployed set of LP modes, as well as Schmidt modes (e.g. also used for step-index fibers), which are usually more difficult to shape with the WMA due to the lack of Canonical symmetries. As such, the generation of LP modes is associated with a dramatic increase in the number of required SLM passages. While recent work on LP mode transmission shows that for each spatial tributary, one passage is required, the limited number of SLM pixels is no longer sufficient. Therefore, in many applications the phasemasks are rather printed on a dielectric mirror, which leads to near-perfect reflection properties, but makes flexibility after fabrication impossible. Here, we restrict the number of reflection passages to as much as $K = 5$ and thereby obtain results that are implementable on a real SLM with limited pixel number. Therefore, we can utilise programmable precompensation approaches using e.g. spatial eigenchannels, as described in Sec. 4.

Fig. 2a shows the WMA result for multiplexing all 45 LP modes the MMF mentioned in Sec. 2 supports, that is $M = N$, using 5 reflection passages. The amplitude of the device’s coupling matrix is shown. Note, that ideal coupling equals a coupling factor of 1, i.e. 0 dB. In this realisation, an average MER of -4.25 dB and IL= -8.28 dB results. Considerable crosstalk of the mode multiplexer is clearly present, which inevitably leads to performance penalty in an SDM system, if no mitigating steps are taken. Apparently, paralleled shaping of 45 modes in such a highly restricted setup is simply too demanding for a 5-passage MPLC and one could expect improvement if the requirements are relaxed.

Let us use less tributaries (i.e. $M < N$) and shape an arbitrary subset of target modes using the WMA. The result for shaping only 5 randomly selected tributaries is shown in Fig. 2b, while the equivalent for 25 tributaries is shown in Fig. 2c. For the 5-tributary case, the average MER equals -2.78 dB and IL= -3.07 dB. In the case of 25 tributaries, an average MER of -2.17 dB and IL= -6.07 dB is achieved. In Fig 2d, boxplots indicate average MER (i.e. $\overline{\text{MER}}$) values under varying number of tributaries. For each data point, we produced 30 WMA runs in each of which a random tributary subset with fixed M is shaped. Examples for the 5 and 25-tributary case are shown in Fig. 2b and Fig. 2c, respectively. It turns out that simply relaxing the shaping effort by reducing the number of tributaries does not provide a universal remedy for high-performance multiplexing using the WMA. The underlying reason for this is the WMA principle, which regulates only the overlap between forward propagating spots and backward propagating target modes. What the WMA does not consider, however, is suppression of coupling to residual modes reducing unwanted crosstalk. Therefore, with a reduced tributary number it is more likely that deviations of the WMA will lead to overlap with a mode other than the target modes. At constant number of degrees of freedom (i.e. SLM pixels), the overlap fidelity to target modes does enhance with decreasing number of tributaries, since the ratio between number of SLM pixels and number of modes increases. Fig. 2e (blue curve) shows the average coupling to target modes. But at the same time, undesired coupling to residual modes also enhances. Fig. 2e (red curve) shows the total coupling to residual modes. Providing a sanity check, the curves in Fig. 2e allow to determine the optimal number of tributaries in terms of MER. Since the target curve is always below the curve indicating coupling to residual modes, the MER is best where the distance between the two curves is smallest. This is the case for about 30 tributaries, which is in line with Fig. 2d.

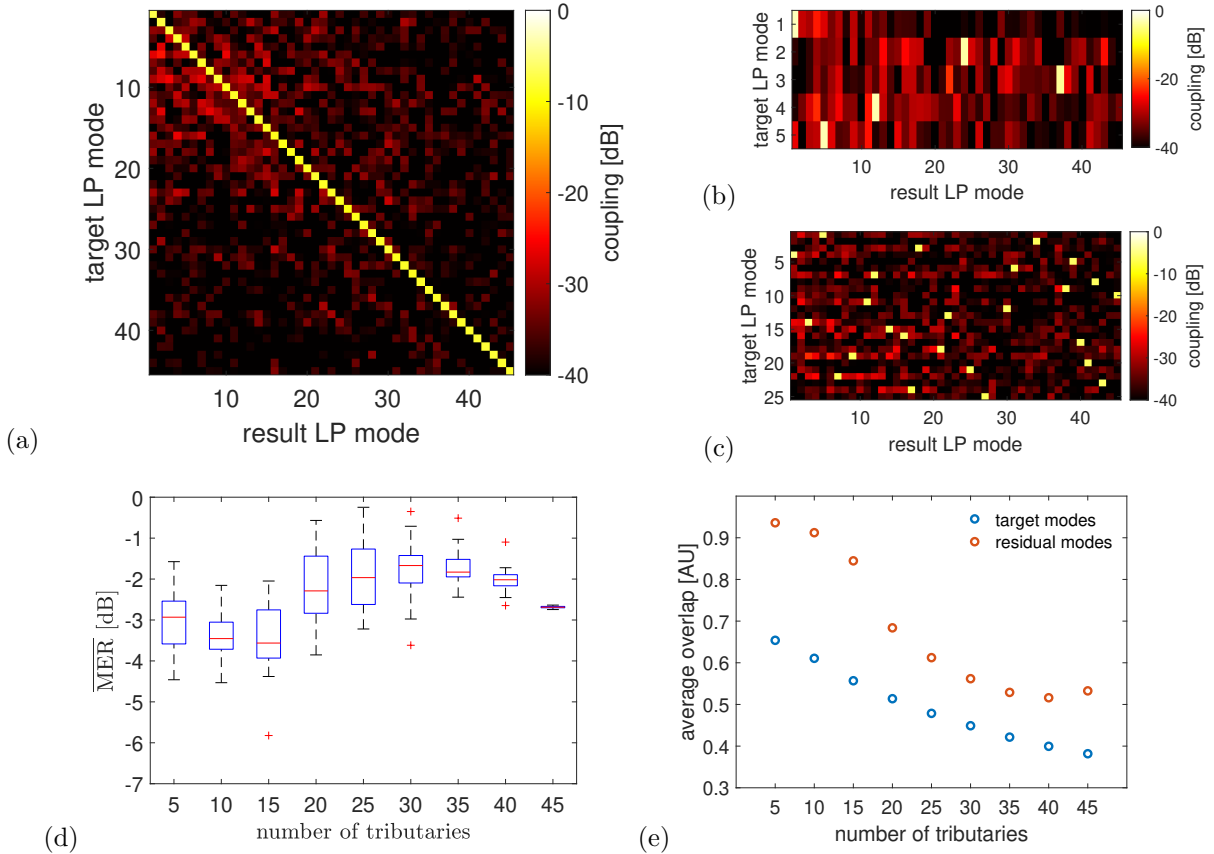


Figure 2: (a) WMA result when shaping all 45 LP modes the MMF supports ($M = N$). (b) WMA result when shaping a random subset of $M = 5$ tributaries out of $N = 45$ LP modes. (c) Same principle as (b), but with a $M = 25$ -tributary subset. (d) average MER box-plotted over different tributary numbers. Each boxplot corresponds to 30 different randomised subsets of the defined number of tributaries. (e) Average overlap to both target and residual modes under varying number of tributaries.

3.2. Dynamic cost function design using direct search

In order to increase the mode multiplexer performance, we propose a novel cost function design tailored to MPLC. We incorporate the wavefront shaping task into a direct search (DS) framework [66, 67, 68]. Using K phasemasks $P(x, y, K)$ resulting from the WMA as initial guess, we randomly select a single phase element p_i of one of the passages and allocate a random phase p_r . After propagating all M input spots $E_{\text{in},m}(x, y)$, $m = 1, 2, \dots, M$ to the final passage, we calculate $\overline{\text{MER}}$, IL as well as the standard deviation σ_{MER} . The phase change will be accepted in the i th iteration, if the cost function is satisfied.

When including $\overline{\text{MER}}$ to the cost, the algorithm does improve the ratio between coupling to target and coupling to residual modes, but it is likely that this goal is achieved by simply increasing the overall loss. Therefore, we also consider IL in the cost function constraining the optimisation algorithm tightly, but also allow deliberate releases. Additionally, we define the maximum standard deviation σ_{MER} among all tributaries as 1 dB. This means, one phase change is accepted, if the $\overline{\text{MER}}$ is improved, the IL is still above the lower bound and the standard deviation σ_{MER} is below 1 dB. Our DS procedure is summarised in Algorithm 1. Additionally, we provide a code example of our method in a repository that is publicly accessible and can be found under Ref. [69].

Figure 3 illustrates an introductory example when using $M = 5$ tributaries out of $N = 45$ LP modes. It shows the progression of both MER and IL plotted over iterations. The initial state provided by the WMA result is characterised with as much as $\overline{\text{MER}} = -2.98$ dB and $\text{IL} = -3.59$ dB (compare Fig. 2d, 5 tributaries). Within the first 250k iterations, the algorithm seeks phase values to reduce cost on both $\overline{\text{MER}}$ and IL.

Algorithm 1 Our DS algorithm

- 1: Initialise input beams $E_{in,m}(x, y)$ $\triangleright m = 1, 2, \dots, M$
 - 2: Initialise phasemasks $P(x, y, K)$ using the WMA as for instance in Ref. [45] $\triangleright K \equiv$ number of passages
 - 3: Define termination criterion $\overline{\text{MER}}_T$ and lower bound IL_{lb}
 - 4: Set $\overline{\text{MER}}_i = -\infty$ dB
 - 5: **while** $\overline{\text{MER}}_i \leq \overline{\text{MER}}_T$ **do** $\triangleright i \equiv$ current iteration
 - 6: Randomly select one phase element $p_i = P(x_r, y_r, K_r)$
 - 7: $P(x_r, y_r, K_r) \leftarrow p_r = 2\pi \cdot \text{rand}()$
 - 8: propagate all beams $E_{in,m}(x, y)$ to last passage
 - 9: calculate $\overline{\text{MER}}_i$ as in (1) and IL_i as in (2), and $\sigma_{\overline{\text{MER}}_i}$
 - 10: **if** $\overline{\text{MER}}_i > \overline{\text{MER}}_{i-1}$ and $\text{IL}_i > \text{IL}_{lb}$ and $\sigma_{\overline{\text{MER}}_i} < 1$ dB **then**
 - 11: $P(x_r, y_r, K_r) = p_r$
 - 12: **else**
 - 13: $P(x_r, y_r, K_r) = p_i$
 - 14: **end if**
 - 15: **end while**
-

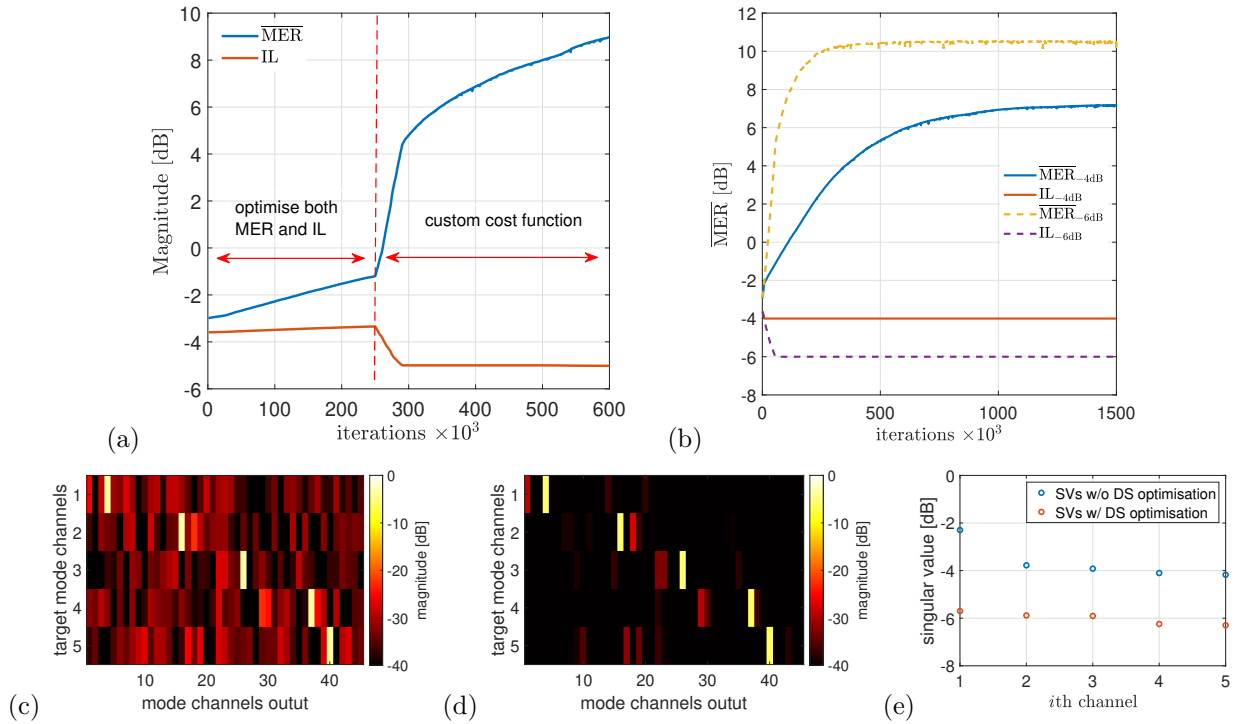


Figure 3: Improving mode multiplexing using DS. When shaping $M = 5$ out of $N = 45$ LP modes using the WMA, we get $\overline{\text{MER}} = -2.98$ dB and $\text{IL} = -3.59$ dB. (a) Now, we use the WMA result as initial guess for DS and put both performance indicators into the cost function. If we try to reduce cost on both $\overline{\text{MER}}$ and IL , the gains are negligible after 250k iterations. The average $\overline{\text{MER}}$ has improved only by 1.7 dB, while the IL improved only 0.2 dB. However, if we deliberately relax the constraints and allow IL deterioration to the minimum of -5 dB, this has a huge impact on $\overline{\text{MER}}$, which improves by 9.2 dB within 250k iterations. Another relaxation to $\text{IL} = -6$ dB improves $\overline{\text{MER}}$ for additional 1 dB within another 100k iterations. (b) Now, we run the algorithm with a constant cost function avoiding local minima. We define a lower bound on IL of as much as -4 dB (blue and orange solid curves), the $\overline{\text{MER}}$ converges at 7.1 dB after 1.5 million iterations and improves by one order of magnitude in total. If we lower the IL threshold to -6 dB (yellow and purple dashed curve), $\overline{\text{MER}}$ improves by as much as 13.5 dB. (c) and (d) show the coupling matrix of the multiplexer before (c) and after (d) DS optimisation corresponding to a lower IL bound of -6 dB (yellow and purple curves in (b)). We find strong suppression of coupling to unwanted modes. (e) Associated singular values of the multiplexer before and after DS optimisation. As targeted, the DS optimisation improves the $\overline{\text{MER}}$ by slightly lowering the IL , i.e. the average singular value. This also lowers the variations among the singular values, that is MDL. In our case, e.g. for the yellow/purple curves in (b) (lower IL bound set to -6 dB), we automatically improve MDL from 0.94 dB calculated for the initial state to 0.29 dB after optimisation.

We observe the gains are vanishing small, since neither $\overline{\text{MER}}$ nor IL improve significantly. While $\overline{\text{MER}}$ has improved by 1.7 dB, the IL improved only 0.2 dB. First, the initial state, that is the WMA result, is already good, yet not ideal. Second, with a limited set of degrees of freedom (i.e. number of SLM pixels) it is impossible to profit on all frontiers simultaneously. Note that a better hologram resolution, i.e. higher number of smaller pixels, could lead to overall improvement, but we restrict our study to the real-world case, where in most cases 8 μm SLM pixels are used.

Now, let us allow an IL deterioration and define a lower bound of -5 dB corresponding to a IL penalty of -1.6 dB. After a few iterations, the algorithm relaxes the IL to the new lower threshold. At the same time, this has great impact on the $\overline{\text{MER}}$ progression which increases by 9.2 dB. If we lower the IL threshold even further to -6 dB, the IL does not exhaust completely, but only relaxes a little. This behaviour indicates, that after running optimisation with specified constraints, the algorithm plateaus in a local minimum. In spite this fact, however, the $\overline{\text{MER}}$ level is raised by another 1 dB. In total, this direct search algorithm with dynamic cost function accomplishes an $\overline{\text{MER}}$ gain by more than one order of magnitude with about 10.2 dB. In exchange, an IL penalty of ≈ 1.6 dB is tolerated.

Fig. 3b shows the case, where we avoid intermediate plateaus and run the algorithm with only one, customised cost function. Allowing a small IL deterioration of -0.4 dB (i.e. lower bound of IL of -4 dB, blue and orange solid curves), the $\overline{\text{MER}}$ reaches 2.6 dB after 250k. Compare this with Fig. 3a, where the $\overline{\text{MER}}$ has reached -1.2 dB after the same number of iterations. In that case, we started with the same initial state, but tried to optimise on both IL $\overline{\text{MER}}$ and achieved an $\overline{\text{MER}}$ improvement of half the slope compared to Fig. 3b. In total, with slight IL deterioration and a relaxed cost function constraint, the $\overline{\text{MER}}$ converges at 7.1 dB after 1.5 million iterations and improves by one order of magnitude. If we lower the IL threshold to even -6 dB (yellow and purple dashed curve), $\overline{\text{MER}}$ improves by as much as 13.5 dB. Figures 3c and d show the two coupling matrices corresponding to the case where we set the lower IL bound to -6 dB, before we start our optimisation (c), and after we terminated it (d). When comparing the two results, we can clearly identify a strong suppression to unwanted modes which proves the improvement in $\overline{\text{MER}}$. Figure 3e shows the singular values for the same case — before and after DS optimisation. We can find that the average singular value, i.e. IL, slightly drops to -6 dB, as initiated. Interestingly, in our simulations we automatically improve on variations among the singular values, i.e. MDL. For instance, in the case where we set the lower IL bound to -6 dB, our optimisation improves MDL from 0.94 dB to 0.29 dB.

4. Transmission of Schmidt modes using direct search

Now we design the same MPLC mode multiplexer using a specialised mode basis and use it for an optimised data transmission. What becomes evident here is the extreme potential of the SLM. Thanks to its programmability, an enormous degree of flexibility is available. It allows to switch the mode base without the need to physically exchange a device, but easily load new phase masks onto its display.

Considering the 45-mode MMF of which we have measured the transmission matrix shown in Fig. 1b, we can derive spatial transmission eigenchannels by means of singular value decomposition (SVD) called Schmidt modes [34] $\text{TM} = U \cdot \Sigma \cdot V^H$. Launched to an MMF with ideal conditions, Schmidt modes enable channel equalisation with zero crosstalk. The Schmidt modes are hidden in the columns of V^H . Each column i is filled with N modal coefficients γ_k representing the k th weight of the corresponding LP mode to the i th Schmidt mode. The field of the i th Schmidt mode, e.g. Ω_i , is then calculated by the weighted sum of all LP modes $\Omega_i = \sum_k^N \gamma_{k,i} \Psi_k$, where Ψ_j indicates the corresponding LP mode field. Fig. 4a shows the first 5 Schmidt modes of the MMF under test. Changing the target basis from LP mode to Schmidt modes allows to adapt the MPLC-based wavefront shaping scheme for a specialised data transmission. We first shape the Schmidt modes using the standard WMA. Next, we use the WMA result as initial guess and carry out DS to reduce cost on $\overline{\text{MER}}$ while not surpassing a lower IL threshold of -6 dB. The $\overline{\text{MER}}$ standard deviation among the Schmidt modes should be within 1 dB. In Fig. 4b the $\overline{\text{MER}}$ progression is plotted for varying number of tributaries M , while Fig. 4c shows the corresponding IL progression. With our dynamic cost function design, DS optimisation achieves 15 dB improvement on $\overline{\text{MER}}$ in exchange for -2.8 dB IL deterioration, by shaping a subset of $M = 5$ Schmidt modes out of the $N = 45$ spatial channels the considered MMF supports. Increase in the number of tributaries will result in degradation of the achievable improvement on $\overline{\text{MER}}$, if the number of SLM pixels and the lower IL limit are kept constant. When shaping 8 Schmidt modes in parallel, the achievable average MER converges at 8.5 dB, while the $\overline{\text{MER}}$ curve converges at 4.5 dB for the 12 Schmidt modes-equivalent. One particular impediment can be attributed to the fact that becomes more difficult to obtain good starting conditions when increasing the number of tributaries. As shown in Fig. 4c, it can be seen that the initial guesses (i.e. the WMA results) are deteriorated with a higher IL, when the number of parallel target Schmidt

modes increases. Consequently, the gain in $\overline{\text{MER}}$ is also hindered to the lower trade-in of IL, given the lower IL threshold remains constant.

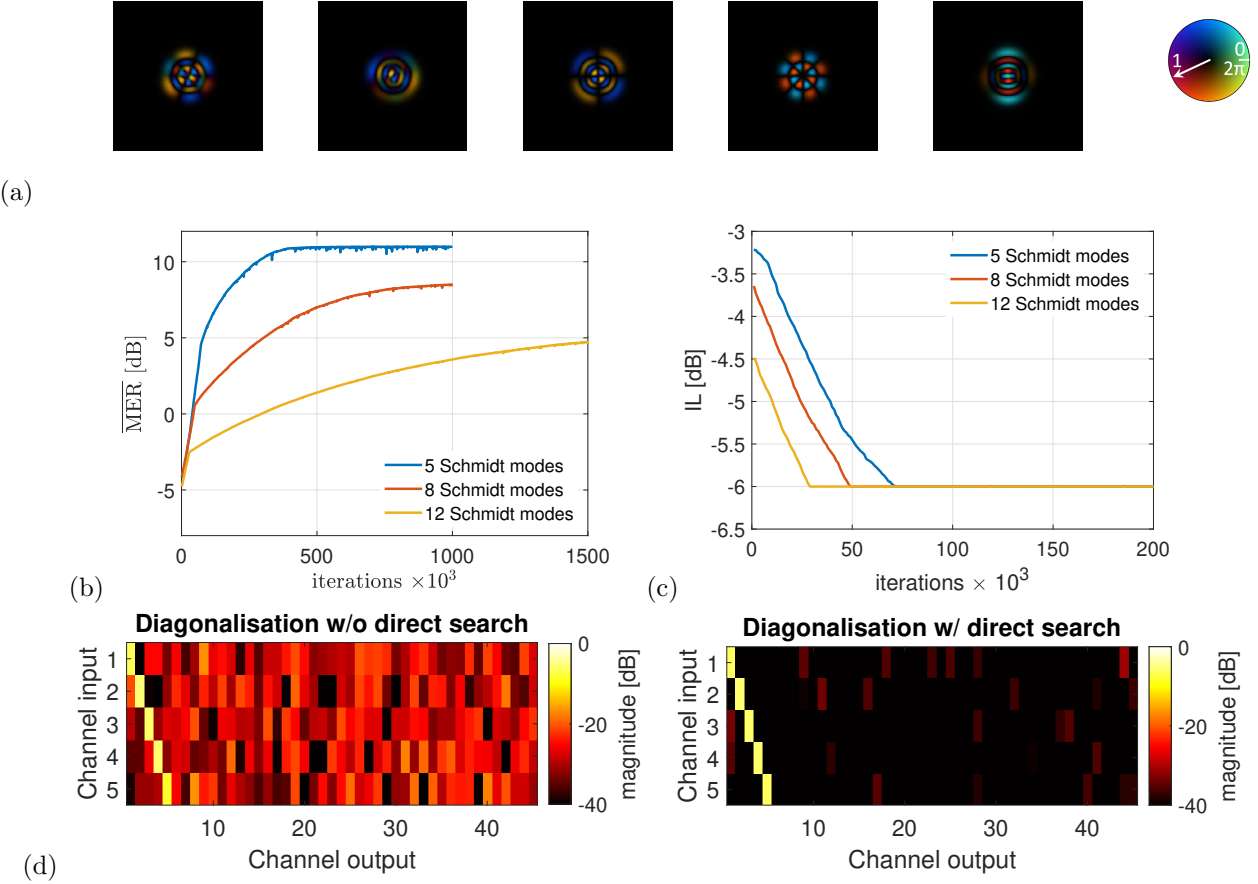


Figure 4: Simulation results on Schmidt mode transmission. (a) shows the first 5 Schmidt modes derived from the measured transmission matrix shown in Fig. 1b. The complex colorbar is shown in the right-hand side. (b) and (c) $\overline{\text{MER}}$ and IL plotted over iterations using our DS method when shaping the first 5, 8 and 12 Schmidt modes at the MMF input, respectively. We use the WMA result as initial guess. We consider the same 5-passage environment as introduced in Section 3 and chose the lower IL limit at -6 dB. When shaping 5 Schmidt modes using our method, we achieve a gain on $\overline{\text{MER}}$ of ≈ 15 dB in exchange for ≈ 2.8 dB IL. In the 5 Schmidt mode-case, the $\overline{\text{MER}}$ curve converges after ≈ 500 k iterations. (d) We simulate channel diagonalisation through an 8 km MMF exciting Schmidt modes at the input. We model the transmission by decomposing the shaped field into the LP mode basis and multiply it with the measured transmission matrix. The resulting vector is multiplied with U^H revealing an equalised eigenchannel. The results for transmitting 5 Schmidt modes using MPLC-based wavefront shaping at the MMF input are shown in the two panels. Left: Schmidt modes are shaped using only WMA. Right: Schmidt modes are shaped with our method.

Next, we compare channel diagonalisation via transmitting and receiving Schmidt modes. We shape the singular eigenchannels derived from the transmission matrix at the MMF input using our DS-based optimisation, as explained in the previous paragraph. Then we simulate transmission by applying mode decomposition to the shaped fields in the LP mode basis matching the basis of our transmission matrix. We then multiply the mode decomposition result with the measured transmission matrix. The transmitted signal becomes equalised by multiplying the conjugate transpose output eigenchannel matrix U^H . Under ideal conditions, this will reveal a diagonal element of Σ the power of which scales with the corresponding singular value. When shaping the first five Schmidt modes (see Fig. 4a) at the MMF input using only the WMA, we recover the channel equalisation result depicted in the left panel of Fig. 4d. In turn, the result shown in the right panel of Fig. 4d is found when shaping the Schmidt modes using our DS-based optimisation procedure. The crosstalk reduction of 15 dB on average is quite significant.

5. Conclusion

We present a computer-generated hologram optimisation algorithm using direct search to enhance programmable optical data transmission through multimode fibres. Our approach comprises a concatenation of phase modulation planes following a multi-plane light conversion path. While traditional multi-plane light conversion configurations rely on the wavefront matching algorithm to calculate the phasemasks, we identify unexploited potential in the phasemask design. By using the wavefront matching result as initial state and applying direct search optimisation, we achieve an overall 15 dB improvement of mode extinction ratio on shaping circularly symmetric linearly polarised modes of the multimode fiber. This reward comes at the expense of a targeted deterioration in insertion loss. However, by imposing a lower bound on insertion loss, we avoid entering undesired parameter territory. Similar to the findings reported in Ref. [50], we observe that relaxing the loss constraints usually yields to higher fidelity, e.g. average mode extinction ratio.

In our simulations, we assume a 5-passage beam transformation with 256×256 pixels per passage, amounting to roughly 327k pixels in total. This setup can be directly implemented on a 1M pixel programmable spatial light modulator. Given such configuration, achieving significant improvements, say 10 dB gain in mode extinction ratio, requires at least 250k computational iterations. The convergence efficiency defined as is the ratio of gain to required iterations substantially depends on the selected constraints — stricter constraints demand more iterations for improvements.

While our method demonstrates clear trade-offs and potential for high-throughput communications, we acknowledge that alternative optimization techniques, such as gradient-based optimisation [70, 50], genetic algorithm [54], deep learning [71, 72, 73] where a recent tutorial can be found in Ref. [74], or Fourier transform-based optimisation [75, 76], may provide similar gains with less computational overhead. Nonetheless, this work highlights the additional opportunities available through careful phasemask design optimisation and its impact on mode extinction ratio.

While our direct search optimisation demonstrates significant improvements over the wavefront matching algorithm, it does not guarantee a globally optimal solution, as both methods are limited by the explored search space and computational constraints. The search for a global optimum in the high-dimensional pixel space remains an open challenge, and further research is required to develop algorithms that are capable of reliably converging to such solutions.

Acknowledgments

We thank David B. Phillips for insightful discussion. This work was supported by the German Federal Ministry of Education and Research (BMBF) with the project 6G-life 6KISK001K, the German Research Foundation (DFG) under grants RO 7348/1-1 and CZ 55/42-2, and the UKRI Future Leaders Fellowship MR/T041218/1.

Disclosures

The authors declare no conflicts of interest.

References

- [1] R.-J. Essiambre, G. Kramer, P. J. Winzer, G. J. Foschini, B. Goebel, *Capacity limits of optical fiber networks*, *Journal of Lightwave Technology* 28 (4) (2010) 662–701.
- [2] D. J. Richardson, *Filling the light pipe*, *Science* 330 (6002) (2010) 327–328.
- [3] D. J. Richardson, J. M. Fini, L. E. Nelson, *Space-division multiplexing in optical fibres*, *Nature photonics* 7 (5) (2013) 354–362.
- [4] B. J. Puttnam, G. Rademacher, R. S. Luís, *Space-division multiplexing for optical fiber communications*, *Optica* 8 (9) (2021) 1186–1203.
- [5] S. Ö. Arık, K.-P. Ho, J. M. Kahn, *Group delay management and multiinput multioutput signal processing in mode-division multiplexing systems*, *Journal of Lightwave Technology* 34 (11) (2016) 2867–2880.
- [6] F. M. Ferreira, C. S. Costa, S. Sygletos, A. D. Ellis, *Semi-analytical modelling of linear mode coupling in few-mode fibers*, *Journal of Lightwave Technology* 35 (18) (2017) 4011–4022.
- [7] R. Ryf, S. Randel, A. H. Gnauck, C. Bolle, A. Sierra, S. Mumtaz, M. Esmaelpour, E. C. Burrows, R.-J. Essiambre, P. J. Winzer, et al., *Mode-division multiplexing over 96 km of few-mode fiber using coherent 6×6 mimo processing*, *Journal of Lightwave technology* 30 (4) (2012) 521–531.
- [8] T. Mori, T. Sakamoto, M. Wada, T. Yamamoto, F. Yamamoto, *Few-mode fibers supporting more than two lp modes for mode-division-multiplexed transmission with mimo dsp*, *Journal of Lightwave Technology* 32 (14) (2014) 2468–2479.
- [9] K.-P. Ho, J. M. Kahn, *Mode-dependent loss and gain: statistics and effect on mode-division multiplexing*, *Optics express* 19 (17) (2011) 16612–16635.
- [10] G. J. Foschini, *Layered space-time architecture for wireless communication in a fading environment when using multi-element antennas*, *Bell Labs Technical Journal* 1 (2) (1996) 41–59. doi:10.1002/bltj.2015.

- [11] K. Shibahara, T. Mizuno, H. Ono, K. Nakajima, Y. Miyamoto, Long-haul dmd-unmanaged 6-mode-multiplexed transmission employing cyclic mode-group permutation, in: *2020 Optical Fiber Communications Conference and Exhibition (OFC)*, 2020, pp. 1–3.
- [12] B. Inan, B. Spinnler, F. Ferreira, D. van den Borne, A. Lobato, S. Adhikari, V. A. J. M. Sleiffer, M. Kuschnerov, N. Hanik, S. L. Jansen, Dsp complexity of mode-division multiplexed receivers, *Opt. Express* 20 (10) (2012) 10859–10869. doi: 10.1364/OE.20.010859. URL <http://opg.optica.org/oe/abstract.cfm?URI=oe-20-10-10859>
- [13] F. M. Ferreira, F. A. Barbosa, Maximizing the capacity of graded-index multimode fibers in the linear regime, *Journal of Lightwave Technology* (2023) 1–8doi: 10.1109/JLT.2023.3324611.
- [14] S. Popoff, G. Lerosey, M. Fink, A. C. Boccarda, S. Gigan, Controlling light through optical disordered media: transmission matrix approach, *New Journal of Physics* 13 (12) (2011) 123021.
- [15] W. Choi, A. P. Mosk, Q.-H. Park, W. Choi, Transmission eigenchannels in a disordered medium, *Physical Review B* 83 (13) (2011) 134207.
- [16] T. Čižmár, K. Dholakia, Exploiting multimode waveguides for pure fibre-based imaging, *Nature communications* 3 (1) (2012) 1027.
- [17] J. Carpenter, B. J. Eggleton, J. Schröder, Complete spatiotemporal characterization and optical transfer matrix inversion of a 420 mode fiber, *Optics letters* 41 (23) (2016) 5580–5583.
- [18] W. Xiong, C. W. Hsu, Y. Bromberg, J. E. Antonio-Lopez, R. Amezcua Correa, H. Cao, Complete polarization control in multimode fibers with polarization and mode coupling, *Light: Science & Applications* 7 (1) (2018) 54.
- [19] M. Mazur, N. K. Fontaine, R. Ryf, H. Chen, D. T. Neilson, M. Bigot-Astruc, F. Achten, P. Sillard, A. Amezcua-Correa, J. Schröder, et al., Characterization of long multi-mode fiber links using digital holography, in: *Optical Fiber Communication Conference, Optical Society of America*, 2019, pp. W4C–5.
- [20] S. Rothe, H. Radner, N. Koukourakis, J. W. Czarske, Transmission matrix measurement of multimode optical fibers by mode-selective excitation using one spatial light modulator, *Applied Sciences* 9 (1) (2019) 195.
- [21] S. Cheng, X. Zhang, T. Zhong, H. Li, H. Li, L. Gong, H. Liu, P. Lai, Nonconvex optimization for optimum retrieval of the transmission matrix of a multimode fiber, *Advanced Photonics Nexus* 2 (6) (2023) 066005. doi: 10.1117/1.APN.2.6.066005. URL <https://doi.org/10.1117/1.APN.2.6.066005>
- [22] J. Zhong, Z. Wen, Q. Li, Q. Deng, Q. Yang, Efficient reference-less transmission matrix retrieval for a multimode fiber using fast Fourier transform, *Advanced Photonics Nexus* 2 (5) (2023) 056007. doi: 10.1117/1.APN.2.5.056007. URL <https://doi.org/10.1117/1.APN.2.5.056007>
- [23] H. Cao, T. Čižmár, S. Turtaev, T. Tyc, S. Rotter, Controlling light propagation in multimode fibers for imaging, spectroscopy, and beyond, *Advances in Optics and Photonics* 15 (2) (2023) 524–612.
- [24] S. G. Leon-Saval, A. Argyros, J. Bland-Hawthorn, Photonic lanterns: a study of light propagation in multimode to single-mode converters, *Optics Express* 18 (8) (2010) 8430–8439.
- [25] N. K. Fontaine, J. Carpenter, S. Gross, S. Leon-Saval, Y. Jung, D. J. Richardson, R. Amezcua-Correa, Photonic lanterns, 3-d waveguides, multiplane light conversion, and other components that enable space-division multiplexing, *Proceedings of the IEEE* 110 (11) (2022) 1821–1834.
- [26] A. Alarcon, J. Argillander, G. Lima, G. B. Xavier, Few-mode-fiber technology fine-tunes losses in quantum communication systems, *Physical review applied* 16 (3) (2021) 034018.
- [27] A. Alarcon, J. Argillander, D. Spiegel-Lexne, G. B. Xavier, Dynamic generation of photonic spatial quantum states with an all-fiber platform, *Optics Express* 31 (6) (2023) 10673–10683.
- [28] A. Velazquez-Benitez, J. Alvarado, G. Lopez-Galmiche, J. Antonio-Lopez, J. Hernández-Cordero, J. Sanchez-Mondragon, P. Sillard, C. Okonkwo, R. Amezcua-Correa, Six mode selective fiber optic spatial multiplexer, *Optics letters* 40 (8) (2015) 1663–1666.
- [29] N. K. Fontaine, R. Ryf, J. Bland-Hawthorn, S. G. Leon-Saval, Geometric requirements for photonic lanterns in space division multiplexing, *Opt. Express* 20 (24) (2012) 27123–27132. doi: 10.1364/OE.20.027123. URL <https://opg.optica.org/oe/abstract.cfm?URI=oe-20-24-27123>
- [30] A. Velázquez-Benítez, J. Antonio-López, J. alvarado zacarias, N. Fontaine, R. Ryf, H. Chen, J. Hernández-Cordero, P. Sillard, C. Okonkwo, S. Leon-Saval, R. Amezcua-Correa, Scaling photonic lanterns for space-division multiplexing, *Scientific Reports* 8. doi: 10.1038/s41598-018-27072-2.
- [31] I. M. Vellekoop, Feedback-based wavefront shaping, *Optics express* 23 (9) (2015) 12189–12206.
- [32] H. Cao, A. P. Mosk, S. Rotter, Shaping the propagation of light in complex media, *Nature Physics* 18 (9) (2022) 994–1007.
- [33] A. D. Gomes, S. Turtaev, Y. Du, T. Čižmár, Near perfect focusing through multimode fibres, *Optics Express* 30 (7) (2022) 10645–10663.
- [34] K.-P. Ho, J. M. Kahn, Linear propagation effects in mode-division multiplexing systems, *Journal of lightwave technology* 32 (4) (2013) 614–628.
- [35] A. P. Mosk, A. Lagendijk, G. Lerosey, M. Fink, Controlling waves in space and time for imaging and focusing in complex media, *Nature photonics* 6 (5) (2012) 283–292.
- [36] M. Kim, Y. Choi, C. Yoon, W. Choi, J. Kim, Q.-H. Park, W. Choi, Maximal energy transport through disordered media with the implementation of transmission eigenchannels, *Nature photonics* 6 (9) (2012) 581–585.
- [37] R. Sarma, A. G. Yamilov, S. Petrenko, Y. Bromberg, H. Cao, Control of energy density inside a disordered medium by coupling to open or closed channels, *Physical review letters* 117 (8) (2016) 086803.
- [38] H. Yılmaz, C. W. Hsu, A. Yamilov, H. Cao, Transverse localization of transmission eigenchannels, *Nature Photonics* 13 (5) (2019) 352–358.
- [39] F. A. Barbosa, F. M. Ferreira, Scaling spatial multiplexing with principal modes, in: *2022 IEEE Photonics Conference (IPC)*, IEEE, 2022, pp. 1–2.
- [40] J. Carpenter, B. J. Eggleton, J. Schröder, Observation of eisensbud-wigner-smith states as principal modes in multimode fibre, *Nature Photonics* 9 (11) (2015) 751–757.
- [41] F. A. Barbosa, F. M. Ferreira, On a scalable path for multimode sdm transmission, *Journal of Lightwave Technology* (2023) 1–10doi: 10.1109/JLT.2023.3308777.
- [42] S. Rothe, K.-L. Besser, D. Krause, R. Kuschmierz, N. Koukourakis, E. Jorswieck, J. W. Czarske, Securing data in multimode

- fibers by exploiting mode-dependent light propagation effects, *Research* 6 (2023) 0065. doi: 10.34133/research.0065. URL <https://spj.science.org/doi/abs/10.34133/research.0065>
- [43] G. Labroille, B. Denolle, P. Jian, P. Genevieux, N. Treps, J.-F. Morizur, Efficient and mode selective spatial mode multiplexer based on multi-plane light conversion, *Optics express* 22 (13) (2014) 15599–15607.
- [44] N. K. Fontaine, R. Ryf, H. Chen, D. Neilson, J. Carpenter, Design of high order mode-multiplexers using multiplane light conversion, in: *2017 European Conference on Optical Communication (ECOC)*, IEEE, 2017, pp. 1–3.
- [45] N. K. Fontaine, R. Ryf, H. Chen, D. T. Neilson, K. Kim, J. Carpenter, Laguerre-gaussian mode sorter, *Nature communications* 10 (1) (2019) 1–7.
- [46] M. Mounaix, N. K. Fontaine, D. T. Neilson, R. Ryf, H. Chen, J. C. Alvarado-Zacarias, J. Carpenter, Time reversed optical waves by arbitrary vector spatiotemporal field generation, *Nature communications* 11 (1) (2020) 1–7.
- [47] N. K. Fontaine, H. Chen, M. Mazur, L. Dallachiesa, K. Kim, R. Ryf, D. Neilson, J. Carpenter, Hermite-gaussian mode multiplexer supporting 1035 modes, in: *Optical Fiber Communication Conference*, Optica Publishing Group, 2021, pp. M3D–4.
- [48] G. Rademacher, B. J. Puttnam, R. S. Luís, T. A. Eriksson, N. K. Fontaine, M. Mazur, H. Chen, R. Ryf, D. T. Neilson, P. Sillard, et al., Peta-bit-per-second optical communications system using a standard cladding diameter 15-mode fiber, *Nature Communications* 12 (1) (2021) 1–7.
- [49] H. Wen, Y. Zhang, R. Sampson, N. K. Fontaine, N. Wang, S. Fan, G. Li, Scalable non-mode selective hermite-gaussian mode multiplexer based on multi-plane light conversion, *Photonics Research* 9 (2) (2021) 88–97.
- [50] H. Kupianskyi, S. A. Horsley, D. B. Phillips, High-dimensional spatial mode sorting and optical circuit design using multi-plane light conversion, *APL Photonics* 8 (2).
- [51] D. Pohle, F. A. Barbosa, F. M. Ferreira, J. Czarske, S. Rothe, Intelligent self calibration tool for adaptive few-mode fiber multiplexers using multiplane light conversion, *Journal of the European Optical Society-Rapid Publications* 19 (1).
- [52] A. Billaud, F. Gomez, D. Allioix, N. Laurenchet, P. Jian, O. Pinel, G. Labroille, Optimal coherent beam combining based on multi-plane light conversion for high throughput optical feeder links, in: *2019 IEEE International Conference on Space Optical Systems and Applications (ICSOS)*, IEEE, 2019, pp. 1–5.
- [53] H. Kupianskyi, S. A. Horsley, D. B. Phillips, All-optically untangling light propagation through multimode fibers, *Optica* 11 (1) (2024) 101–112.
- [54] R. Fickler, F. Bouchard, E. Giese, V. Grillo, G. Leuchs, E. Karimi, Full-field mode sorter using two optimized phase transformations for high-dimensional quantum cryptography, *Journal of Optics* 22 (2) (2020) 024001.
- [55] U. G. Bütaitė, H. Kupianskyi, T. Čizmár, D. B. Phillips, How to build the “optical inverse” of a multimode fibre, *Intelligent Computing*.
- [56] X. Lin, Y. Rivenson, N. T. Yardimci, M. Velí, Y. Luo, M. Jarrahi, A. Ozcan, All-optical machine learning using diffractive deep neural networks, *Science* 361 (6406) (2018) 1004–1008.
- [57] H. Zhou, J. Dong, J. Cheng, W. Dong, C. Huang, Y. Shen, Q. Zhang, M. Gu, C. Qian, H. Chen, et al., Photonic matrix multiplication lights up photonic accelerator and beyond, *Light: Science & Applications* 11 (1) (2022) 1–21.
- [58] M. Yıldırım, N. U. Dinc, I. Oguz, D. Psaltis, C. Moser, Nonlinear processing with linear optics, *Nature Photonics* (2024) 1–7.
- [59] Y. Sakamaki, T. Saida, T. Hashimoto, H. Takahashi, New optical waveguide design based on wavefront matching method, *Journal of lightwave technology* 25 (11) (2007) 3511–3518.
- [60] P. Tsang, T.-C. Poon, Y. Wu, Review of fast methods for point-based computer-generated holography, *Photonics Research* 6 (9) (2018) 837–846.
- [61] S. Rothe, P. Daferner, S. Heide, D. Krause, F. Schmieder, N. Koukourakis, J. W. Czarske, Benchmarking analysis of computer generated holograms for complex wavefront shaping using pixelated phase modulators, *Optics Express* 29 (23) (2021) 37602–37616.
- [62] N. K. Fontaine, R. Ryf, H. Chen, D. T. Neilson, K. Kim, J. Carpenter, Laguerre-gaussian mode sorter supplemental information.
- [63] D. Gloge, Weakly guiding fibers, *Applied optics* 10 (10) (1971) 2252–2258.
- [64] A. Snyder, *Optical waveguide theory* (1983).
- [65] A. E. Siegman, Hermite-gaussian functions of complex argument as optical-beam eigenfunctions, *JOSA* 63 (9) (1973) 1093–1094.
- [66] M. A. Seldowitz, J. P. Allebach, D. W. Sweeney, Synthesis of digital holograms by direct binary search, *Applied optics* 26 (14) (1987) 2788–2798.
- [67] M. Clark, R. Smith, A direct-search method for the computer design of holograms, *Optics Communications* 124 (1-2) (1996) 150–164.
- [68] P. J. Christopher, R. Mouthaan, G. S. Gordon, T. D. Wilkinson, Holographic predictive search: Extending the scope, *Optics Communications* 467 (2020) 125701.
- [69] S. Rothe, F. M. Ferreira, Direct search optimisation algorithm for mode multiplexers (2024). URL <https://github.com/StefRot1992/direct-search-mode-multiplexer>
- [70] N. Barré, A. Jesacher, Holographic beam shaping of partially coherent light, *Optics Letters* 47 (2) (2022) 425–428.
- [71] P. Buske, A. Völl, M. Eisebitt, J. Stollenwerk, C. Holly, Advanced beam shaping for laser materials processing based on diffractive neural networks, *Optics express* 30 (13) (2022) 22798–22816.
- [72] B. Mills, J. A. Grant-Jacob, M. Praeger, R. W. Eason, J. Nilsson, M. N. Zervas, Single step phase optimisation for coherent beam combination using deep learning, *Scientific Reports* 12 (1) (2022) 5188.
- [73] P. Buske, O. Hofmann, A. Bonnhoff, J. Stollenwerk, C. Holly, High fidelity laser beam shaping using liquid crystal on silicon spatial light modulators as diffractive neural networks, *Optics Express* 32 (5) (2024) 7064–7078.
- [74] B. Hadad, S. Froim, E. Yosef, R. Giryas, A. Bahabad, Deep learning in optics—a tutorial, *Journal of Optics*.
- [75] C. Chang, J. Xia, L. Yang, W. Lei, Z. Yang, J. Chen, Speckle-suppressed phase-only holographic three-dimensional display based on double-constraint gerchberg-saxton algorithm, *Applied optics* 54 (23) (2015) 6994–7001.
- [76] Y. Hayasaki, R. Onodera, K. Kumagai, S. Hasegawa, Automatic generation of a holographically shaped beam in an actual optical system for use in material laser processing, *Optics Express* 31 (2) (2023) 1982–1991.